Multiband Superconductivity in Co-doped $SrFe_2As_2$ Investigated by Local Magnetic Imaging

W M Desoky[1,2], S J Bending[1], S E Sebastian[3]

[1]Department of Physics, University of Bath, Claverton Down, UK

[2]Department of Physics, Zagazig University, Egypt.

[3]Quantum Matter Group, Cavendish Laboratory, Madingley Road, Cambridge CB3 0HE

Abstract

High resolution scanning Hall probe microscopy and Hall magnetometry have been used to investigate the magnetic properties of superconducting Co-doped $SrFe_{2-x}Co_xAs_2$ single crystals. We resolve rather disordered field-cooled vortex structures at all values of applied field studied due to the strong vortex pinning arising from substitution of Fe with Co. We have fitted the profiles of well-isolated vortices as a function of temperature to extract *mesoscopic* estimates of the temperature dependence of the magnetic field penetration depth, λ. These data were then used to calculate the superfluid density (ρ_s) over the full temperature range and fitted to a two band α-model with two full gaps. The results suggest that the superfluid density is shared almost equally between hole and electron pockets and that the larger (electron pocket) gap appears to have an approximately isotropic s-wave order parameter. Displacements of the vortices from an ideal triangular lattice have been used to estimate the low field pinning forces which are several orders of magnitude smaller than values estimated by other means on similar superconducting crystals.

Introduction

The discovery of superconductivity at 26 K in the Fe-based system $LaFeAsO_{1-x}F_x$ [1] has led to intense worldwide research activity targeted at understanding and optimising the properties of these compounds. Attempts to increase the superconducting transition temperature by replacing La with other rare earth ions were successful in raising T_c to 55 K in $SmFeAsO_{0.9}F_{0.1}$ [2]. In addition to this '1111' ROFeAs (R = La, Ce, Pr, Nd, Sm) structure family of oxypnictide superconductors, several other families have been discovered based on FeAs layers including the ternary '122' compounds AFe_2As_2 with the $ThCr_2Si_2$ crystal structure (A = Sr, Ba, Ca). The parent '122' compounds are bad metals and exhibit tetragonal-to-orthorhombic structural phase transitions at quite high temperatures that are closely associated with the formation of a static spin-density wave [3] (T_o = 205K in $SrFe_2As_2$ [4]). Hole [5] or electron [6] doping has been shown to suppress the spin and structural transitions when the ground state becomes superconducting. Here we investigate electron-doped $SrFe_{2-x}Co_xAs_2$ single crystal samples in which the existence of superconductivity has been observed in both the antiferromagnetic (orthorhombic) phase as well as in the paramagnetic (tetragonal) phase [7]. In this material the parent compound can also be driven superconducting with T_c as high as 27K by the application of hydrostatic pressure [4, 8], and the T-P phase diagram typically shows a strong similarity to the T-x phase diagram for hole and electron doping.

Band structure calculations based on the local density approximation indicate that multiple bands contribute to the Fermi surface in the '122' compounds which contain at least two hole and two electron pockets. ARPES measurements [9-13] show isotropic nodeless gaps with two distinct energies on different parts of the Fermi surface and there is growing evidence for an s± pairing state where the sign of the order parameter is reversed on hole and electron pockets [14-17]. This s± two-band picture is, however, only an approximate effective theory and clearly does not take into account the true band structure with up to five bands intersecting the Fermi surface. Hence we are far from having a complete understanding of the physics of these fascinating materials.

The superconducting gap structure is usually probed via the excitation rate of quasiparticles, which can be readily measured by studying the temperature dependence of the magnetic field penetration depth, $\lambda(T)$. Such measurements have the advantage that they directly probe the

superfluid density, $\rho_\sigma(T)/\rho_\sigma(0)=\lambda(0)^2/\lambda(T)^2$, which is a measure of the number of electrons in the superconducting state and contains information about the temperature-dependent superconducting gaps [18-23]. Here we use high resolution scanning Hall probe magnetic imaging of individual vortices to measure the *local* temperature-dependent magnetic penetration depth, $\lambda(T)$, in high quality $SrFe_{2-x}Co_xAs_2$ single crystals. A multiple gap fitting procedure has then been used to model the calculated superfluid density which yields insights into the number and nature of superconducting gaps at the Fermi surface.

The Fe-based superconductors initially appeared very promising for high current applications as they exhibit high critical magnetic fields with relatively low crystalline anisotropy, and the suggested s± order parameter should favour strong current flow across grain boundaries, in contrast to the situation in the d-wave cuprate superconductors. In practice, however, the pnictides have also been shown to suffer from intrinsically low critical currents [24-26] and huge magnetic relaxation [24], and there is growing evidence that grain boundaries again represent weak channelling planes for vortices. In addition, nearly all imaging experiments have shown a highly disordered vortex lattice in single crystal samples. Recently, however, it has been shown that the introduction of columnar defects via heavy ion irradiation can considerably enhance J_c and strongly suppresses vortex creep rates [26, 27]. Hence, a better understanding of vortex matter and pinning potentials in these materials could yet prove important to enable future high current applications.

Experimental Method

High resolution scanning Hall probe microscopy (SHPM) has been used to perform the local magnetic imaging presented here. SHPM is a non-invasive magnetic imaging technique whereby a sub-micron Hall effect sensor is scanned just above the surface of the sample to be imaged in order to generate two-dimensional maps of the local magnetic induction. Figure 1a shows a schematic of our microscope which is a modified low temperature STM in which the usual tunnelling tip at the end of the piezoelectric scanner tube has been replaced by a microfabricated GaAs/AlGaAs heterostructure chip. Electron beam lithography and wet chemical etching were used to define a 0.8 μm Hall probe in the two-dimensional electron gas approximately 5 μm from the corner of a deep mesa etch, which was

coated with a thin Au layer to act as an integrated STM tip (figure 1b). The sample sits on an inertial motor and is first approached towards the sensor until tunnelling is established and then retracted about 100-200 nm allowing rapid scanning. The Hall probe makes an angle of about 1° with the sample plane so that the STM tip is always the closest point to the surface, and each 2D map of magnetic induction is usually divided into 128×128 pixels. If required, several images (~10) are averaged frame-by-frame to suppress low frequency noise arising from the Hall sensor. A more detailed description of the instrument and scanning technique is given elsewhere [28]. Although the spatial resolution of SHPM is only modest, being limited by a combination of the geometrical Hall sensor size and the sample/sensor spacing, it does have a number of advantages over other magnetic imaging techniques. It can be used over a very broad range of temperatures in the presence of large external magnetic fields, and produces a quantitative measure of one component of the local magnetic induction, B_z.

The sample studied here was a high quality single crystal of the Co-doped '122' superconductor $SrFe_{2-x}Co_xAs_2$ (x~0.11) which was prepared by the flux growth technique [4, 29] using starting elements of greater than 99.99% purity and a FeAs self-flux. The inset to figure 2 shows a typical 'local' magnetisation loop ($M_l=B_z-H_z$) at T=12.5K that was captured by parking the Hall sensor a few hundred nanometres above the surface of the crystal and sweeping the applied magnetic field around a minor hysteresis loop between H=±70 Oe. The height of this loop, ΔM, averaged at H_z=+/-30Oe is a measure of the diamagnetic screening (critical current) and is plotted in the main graph on figure 2 as a function of temperature. We find that ΔM falls steeply towards zero as T~13.5K is approached from below, and a linear extrapolation of the data in this region suggest T_c=13.65±0.05K. ΔM does, however, exhibit a small tail extending up to about 15K. Since $SrFe_2As_2$ is known to be weakly paramagnetic in the normal state [30] this residual diamagnetism must arise due to weak sample inhomogeneity and the presence of small regions with slightly higher critical temperature.

Figure 3 illustrates vortex-resolved SHPM images for our $SrFe_2As_2$ single crystal after field-cooling to T=8K from the normal state (T>15K) in small perpendicular applied magnetic fields

between -4Oe and +7Oe. Under these conditions the temperature-dependent scan range of the piezoelectric tube is ~8μm×8μm and, in the absence of any diamagnetic screening, we would expect to generate about 3 vortices per Oersted on average. In practice, although changes in number and sign of vortices as a function of field are qualitatively what one would expect, the actual number of vortices seen is considerably less than this estimate indicating quite strong magnetic screening. In addition the true magnetic field zero is offset by about ~+1.3Oe due to the earth's field as well as stray fields from nearby ferrous materials.

In figure 4 we make a quantitative comparison between our measured vortex profiles and a modified variational vortex model due to Clem [31]. The sample was field-cooled in H_z=+1Oe from above T_c which gave rise to one well-isolated vortex as illustrated in the inset to figure 4a. The first image was captured at T=5K, and the temperature raised and the sample reimaged at a number of temperatures up to T_c. In doing so care was taken to scan at the same height at each new temperature and to account for the temperature-dependent scan range of the piezoelectric scanner tube. The vortex profiles were fitted to the following expression

$$B_j = \frac{1}{w^2}\int_{\frac{-w}{2}}^{\frac{w}{2}}\int_{x_j-\frac{w}{2}}^{x_{x+}+\frac{w}{2}}\frac{\phi_0}{2\pi}\int_0^{\infty}\left(\frac{(\sqrt{q^2+\lambda^{-2}})}{(\sqrt{q^2+\lambda^{-2}}+q)}\right)\frac{K_1(\sqrt{q^2+\lambda^{-2}}\,\xi_v)\exp(-qz)J_0(q\sqrt{x^2+y^2})qdqdxdy}{(\sqrt{q^2+\lambda^{-2}})\lambda K_1(\frac{\xi_v}{\lambda})}, \quad (1)$$

where $\xi_v(T) = 2.5nm/(1-T/T_c)^{1/2}$ is a variational coherence length, $\lambda(T)$ is the penetration depth, z is the sensor scan height measured from the surface of the sample and ϕ_0 is the flux quantum. The first term in brackets inside the integral is a correction term proposed by Kirtley *et al.* [32] that accounts for screening at the sample surface. With two fit parameter, λ(T) and z, the agreement between the model and our experimental data is excellent as illustrated in figure 4a at four different characteristic temperatures for λ(0)=315nm and z=1.81μm. This fitted scan height is somewhat larger than we would generally expect and probably reflects that fact that the sensor tilt angle is somewhat greater than 1^o in these measurements. However, the excellent fit quality allows us to extract values

of the temperature-dependent penetration depth, λ(T), at each measurement temperature and the values of $\Delta\lambda(T)= \lambda(T)- \lambda(0)$ obtained are plotted in Fig. 4b.

Following a procedure described by Luan *et* al. [33] to model MFM data on $Ba(Fe_{0.95}Co_{0.05})_2As_2$ single crystals, we use the results of Fig. 4 to calculate the superfluid density, $\rho_s(T)/\rho_s(0)=\lambda(0)^2/\lambda(T)^2$, and fit it to a two band α-model with two full gaps [34, 35] which is a simplified version of a self-consistent model due to Kogan *et al*. [36]. The α-model assumes that $\rho_s(T)=p\rho_1(T)+(1-p)\rho_2(T)$, where $\rho_{1,2}(T)$ are the superfluid densities in the two different bands and p takes account of the relative contribution from each. The individual superfluid densities have been calculated assuming the following expression for isotropic s-wave pairing [18]

$$\rho_i(T) = 1 - \frac{1}{2kT}\int_0^\infty \cosh^{-2}\left(\frac{\sqrt{\varepsilon^2+\Delta_i(T)^2}}{2kT}\right)d\varepsilon\,. \qquad (2)$$

Here the gap was assumed to be given by

$$\Delta_i(T) = \Delta_i(0)\tanh\left[\frac{\pi kT_c}{\Delta_i(0)}\sqrt{a_i\left(\frac{T_c}{T}-1\right)}\right]\,, \qquad (3)$$

where a_i is a characteristic parameter that reflects the specific pairing state (e.g., a_i=1 for isotropic s-wave pairing). Figure 5 shows the experimentally measured dependence of the superfluid density (points with error bars) along with the fits to our two-band α-model (solid line) with Δ_1=4.8kT_c, Δ_2=2.0kT_c, p=0.49, and a_1=0.94, a_2=1. Gap values for the two bands were taken from the results of point contact spectroscopy [37], a_2 was assumed to be unity, and the values of a_1 and p were extracted from an automated fitting routine. Also shown in Fig. 5 is the result of a one band fit (dashed line) with a=0.92 and Δ=2.81kT_c for comparison.

Finally in Figure 6 we investigate the microscopic vortex pinning landscape in our Co-doped $SrFe_2As_2$ single crystal by comparing images captured after repeatedly field-cooling from above T_c to T=8K in the same applied field of H_z=+5Oe. Here images captured after three successive cooling cycles are shown and we note that, although each image contains approximately the same number of vortices, the local vortex structure (as illustrated by the superimposed net) is qualitatively different in

each case. This suggests that these vortex structures are stabilising in the presence of quite a high density of microscopic pinning sites which leads to a different structural realisation each time.

Discussion

Figure 5 reveals that the two-gap model is a better fit to the low temperature superfluid density than the one-gap model, although the difference is clearly quite small. It is generally assumed that the smaller gap is located on the hole pockets at the Γ-point, and we see that in this case the superfluid density appears to be fairly equally shared between these hole pockets and electron pockets at the M-points. Making the usual assumption that the hole gap is isotropic s-wave (a_2=1), our fitted value of a_1=0.94 is rather close to unity within our experimental errors indicating that we also appear to have an approximately isotropic s-wave electron order parameter with no clear evidence for nodes. However, this conclusion needs to be examined more critically since we find that the temperature dependence of the fitted penetration depth is sensitive to the value of λ(0) which is used as an input parameter to calibrate the scan height, z, at low temperature. To explore this point further we have repeated the same fitting routine described above for λ(0)=315+50nm and λ(0)=315-50nm and extracted values of z=1.76μm and z=1.86μm respectively. We find that the error introduced by our choice of λ(0) is cancelled to a significant degree when we plot the ratio $(\lambda(0)/\lambda(T))^2$ and, while the fitted weighting of superfluid density, *p*, for the two bands does depend somewhat on this choice, the fit parameter a_1 is rather insensitive to it. Hence we can conclude with some confidence that the electron pockets are indeed behaving with something close to an isotropic s-wave order parameter.

The disordered vortex structures observed in our images (c.f., Figure 6), which deviate strongly from an ideal triangular lattice, are expected due to pinning arising from the direct substitution (doping) of Fe with Co in the superconducting planes of our samples. Fig. 6 reveals that the vortices adopt quite different disordered structures upon sequentially field cooling at H=5Oe, indicating that the vortices are being pinned in a reasonably dense distribution of reasonably equal strength pinning centres rather being trapped by just a handful of very strong pinning centres. Hence there are a many more-or-less equivalent energy vortex

structures that can nucleate on cooling. In practice we have assumed that the force per unit length between a pair of vortices takes the form [38]

$$\vec{f}^{v-v}(r) = \frac{2\phi_0^2}{4\pi\mu_0\lambda^3} K_1\left(\frac{r}{\lambda}\right)\hat{r} \cong \frac{2\phi_0^2}{4\pi\mu_0\lambda^3}\sqrt{\frac{\pi\lambda}{2r}} exp\left(-\frac{r}{\lambda}\right)\hat{r}, \qquad (4)$$

where $K_1(x)$ is a modified Bessel function of the third kind, r is the separation of the vortices and $\hat{r}$ is a unit vector along the line joining the two vortex cores. We have estimated the vortex-vortex distances from images like those in Fig. 6 and calculated the net force on a centrally positioned vortex due to its nearest neighbours. This resultant force is typically in the range f_p~2-10×10^{-9} N/m, and we take this to represent a lower bound for the low field pinning force in our crystals. Using the relationship $j_c \approx f_p/\phi_0$ this translates into a critical current density in the range 1-5×10^2 A/cm^2, considerably smaller than other values estimated from high field magnetisation studies (e.g., j_c~2.6×10^5 A/cm^2 as estimated for $Ba(Fe_{0.93}Co_{0.07})_2As_2$ by a range of independent techniques at 5K [24]). It is, however, known from Bitter decoration studies that the vortex structure freezes in during field-cooling at a temperature T*~(0.8-0.9) T_c at which the typical strength of pinning sites has grown to the point where vortices can no longer escape [39]. Hence, what one is probing in low temperature imaging is the vortex structure that was in equilibrium with the pinning landscape at the much higher temperature of T* when pinning potentials are much shallower and the penetration depth much longer. Consequently our estimate of local pinning force for well-isolated vortices probably corresponds to a temperature of T*~12K and should not be directly compared with low temperature values of j_c. Moreover, isothermal magnetisation measurements on Co-doped 122 single crystals are known to exhibit a non-monotonic fishtail shape and, on the basis of magnetic relaxation measurements, have been shown [24] to be consistent with collective pinning and creep models with a crossover to a plastic creep regime at fields above the position of the maximum in the fishtail magnetisation. Hence we would also expect the pinning force measured at very low fields, where vortices interact very weakly, to be significantly smaller than higher field measurements where collective pinning effects are becoming important.

Conclusions

We have fitted the temperature dependent vortex profiles in single crystals of the $SrFe_{2-x}Co_xAs$ (x=0.11) Fe-pnictide superconductor to extract the temperature dependence of the superfluid density. Our data fits well to a two band α-model with two full gaps. Our fit parameters suggest that the superfluid density is shared almost equally between hole and electron pockets and that the larger (electron pocket) gap appears to have an approximately isotropic s-wave order parameter. Displacements of the vortices from an ideal triangular lattice have been used to estimate the low field pinning forces. These translate to values of the critical current that are several orders of magnitude smaller than values estimated by other means on similar superconducting crystals, reflecting the importance of collective pinning effects at high fields.

This work was supported by the Engineering and Physical Sciences Research Council (EPSRC) in the U.K. under grants number EP/D034264/1 and EP/E039944/1.

References

[1] Kamihara Y, Watanabe T, Hirano M and Hosono H 2008 *Journal of the American Chemical Society* **130** 3296

[2] Ren Z A, Che G C, Dong X L, Yang J, Lu W, Yi W, Shen X L, Li Z C, Sun L L, Zhou F and Zhao Z X 2008 *Europhysics Letters* **83** 17002.

[3] Sasmal K, Lv B, Lorenz B, Guloy A M, Chen F, Xue Y Y and Chu C W 2008 *Physical Review Letters* **101** 107007.

[4] Gillett J, Das S D, Syers P, Ming A K T, Espeso J I, Petrone C M, Sebastian S E 2010 *arxiv 1005.1330*

[5] Rotter M, Tegel M and Johrendt D 2008 *Physical Review Letters* **101** 107006.

[6] Sefat A S, Jin R, McGuire M A, Sales B C, Singh D J and Mandrus D 2008 *Physical Review Letters* **101** 117004.

[7] Kim J S, Khim S, Yan L, Manivannan N, Liu Y, Kim I, Stewart G R and Kim K H 2009 *J. Phys.: Condens. Matter* **21** 102203

[8] Wu G, Liu R H, Chen H, Yan Y J, Wu T, Xie Y L, Ying J J, Wang X F, Fang D F and Chen X H 2008 *Europhysics Letters* **84** 27010.

[9] Terashima K, Sekiba Y, Bowen J H, Nakayama K, Kawahara T, Sato T, Richard P, Xu Y M, Li L J, Cao G H, Xu Z A, Ding H and Takahashi T 2009 *Proceedings of the National Academy of Sciences* **106** 7330.

[10] Nakayama K, Sato T, Richard P, Xu Y M, Sekiba Y, Souma S, Chen G F, Luo J L, Wang N L, Ding H and Takahashi T 2009 *Europhysics Letters* **85** 67002.

[11] Ding H, Richard P, Nakayama K, Sugawara K, Arakane T, Sekiba Y, Takayama A, Souma S, Sato T, Takahashi T, Wang Z, Dai X, Fang Z, Chen G F, Luo J L and Wang N L 2008 *Europhysics Letters* **83** 47001.

[12] Evtushinsky D V, Inosov D S, Zabolotnyy V B, Viazovska M S, Khasanov R, Amato A, Klauss H H, Luetkens H, Niedermayer C, Sun G L, Hinkov V, Lin C T, Varykhalov A, Koitzsch A, Knupfer M, Büchner B, Kordyuk A A and Borisenko S V 2009 *New Journal of Physics* **11** 055069.

[13] Evtushinsky D V, Inosov D S, Zabolotnyy V B, Koitzsch A, Knupfer M, Büchner B, Viazovska M S, Sun G L, Hinkov V, Boris A V, Lin C T, Keimer B, Varykhalov A, Kordyuk A A and Borisenko S V 2009 *Physical Review B* **79** 054517.

[14] Mazin I I, Singh D J, Johannes M D and Du M H 2008 *Physical Review Letters* **101** 057003.

[15] Kondo T, Santander-Syro A F, Copie O, Liu C, Tillman M E, Mun E D, Schmalian J, Bud'ko S L, Tanatar M A, Canfield P C and Kaminski A 2008 *Physical Review Letters* **101** 147003.

[16] Hanaguri T, Niitaka S, Kuroki K and Takagi H 2010 *Science* **328** 5977.

[17] Shishido H, Bangura A F, Coldea A I, Tonegawa S, Hashimoto K, Kasahara S, Rourke P M C, Ikeda H, Terashima T, Settai R, Ōnuki Y, Vignolles D, Proust C, Vignolle B, McCollam A, Matsuda Y, Shibauchi T and Carrington A 2010 *Physical Review Letters* **104** 057008.

[18] Prozorov R and Giannetta R W 2006 *Supercond. Sci. Technol* **19** R41.

[19] Hardy W N, Bonn D A, Morgan D C, Liang R and Zhang K 1993 *Physical Review Letters* **70** 3999.

[20] Hashimoto K, Shibauchi T, Kasahara S, Ikada K, Tonegawa S, Kato T, Okazaki, R, van der Beek C J, Konczykowski M, Takeya H, Hirata K, Terashima T and Matsuda Y 2009 *Physical Review Letters* **102** 207001.

[21] Hashimoto K, Yamashita M, Kasahara S, Senshu Y, Nakata N, Tonegawa S, Ikada K, Serafin A, Carrington A, Terashima T, Ikeda H, Shibauchi T and Matsuda Y 2010 *Physical Review B* **81** 220501.

[22] Martin C, Gordon R T, Tanatar M A, Kim H, Ni N, Bud'ko S L, Canfield P C, Luo H, Wen H H, Wang Z, Vorontsov A B, Kogan V G and Prozorov R 2009 *Physical Review B* **80** 020501.

[23] Gordon R T, Martin C, Kim H, Ni N, Tanatar M A, Schmalian J, Mazin I I, Bud'ko S L, Canfield P C and Prozorov R *2009 Physical Review B* **79** 100506.

[24] Prozorov R, Ni N, Tanatar M A, Kogan V G, Gordon R T, Martin C, Blomberg E C,

Prommapan P, Yan J Q, Bud'ko S L and Canfield P C 2008 *Physical Review B* **78** 224506.

[25] Yamamoto A, Jaroszynski J, Tarantini C, Balicas L, Jiang J, Gurevich A, Larbalestier D C, Jin R, Sefat A S, McGuire M A, Sales B C, Christen D K and Mandrus D 2009 *Applied Physics Letters* **94** 062511.

[26] Nakajima Y, Tsuchiya Y, Taen T, Tamegai T, Okayasu S and Sasase M 2009 *Physical Review B* **80** 012510.

[27] Prozorov R, Tanatar M A, Shen B, Cheng P, Wen H H, Bud'ko S L and Canfield, P C 2010 *Physical Review B* **82** 180513.

[28] Oral A, Bending S J and Henini M 1996 *Applied Physics Letter* **69** 1324.

[29] Loudon J C, Bowell C J, Gillett J, Sebastian S E and Midgley P A 2010 *Physical Review B* **81** 214111.

[30] Prozorov R, Tanatar M A, Roy B, Ni N, Bud'ko S L and Canfield P C, Hua J, Welp U and Kwok W K 2010 *Phys. Rev. B* **81** 094509.

[31] Clem J R 1975 *J. Low Temp. Phys.* **18** 427

[32] Kirtley J R, Kallin C, Hicks C W, Kim E A, Liu Y, Moler K A, Maeno Y and Nelson K D 2007 *Physical Review B* **76** 014526.

[33] Luan L, Auslaender O M, Lippman T M, Hicks C W, Kalisky B, Chu J H, Analytis J G, Fisher I R, Kirtley J R and Moler K A 2010 *Physical Review B* **81** 100501.

[34] Fletcher J D, Carrington A, and Taylor O J , Kazakov S M and Karpinski J 2005 *Physical Review Letter* **95** 097005.

[35] Bouquet F, Wang Y, Fisher R A, Hinks D G, Jorgensen J D, Junod A and Phillips N E 2001 *Europhysics Letters* **56** 856.

[36] Kogan V G, Martin C and Prozorov R 2009 *Physical Review B* **80** 014507.

[37] Hunt C, Arham H, Park W, Greene L, Gillett J and Sebastian S Abstract: X23.00013, *Bulletin of the American Physical Society* **56** 1 2011

[38] Huebener R 2003 Magnetic flux structures in superconductors 2nd edn. (Springer) p 63

[39] Grigorieva I V 1994 *Superconductor Science and Technology* **7** 161.

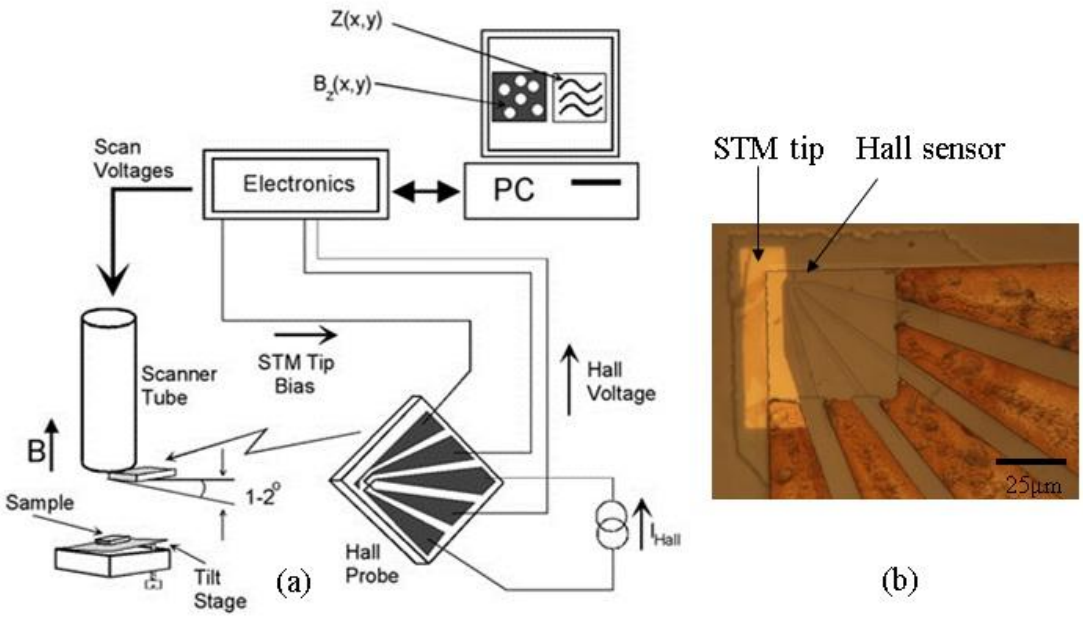

Figure 1(a) Schematic of the scanning Hall probe microscope system. (b) (Colour on-line) Optical micrograph of a typical magnetic sensor showing STM tip and active Hall probe.

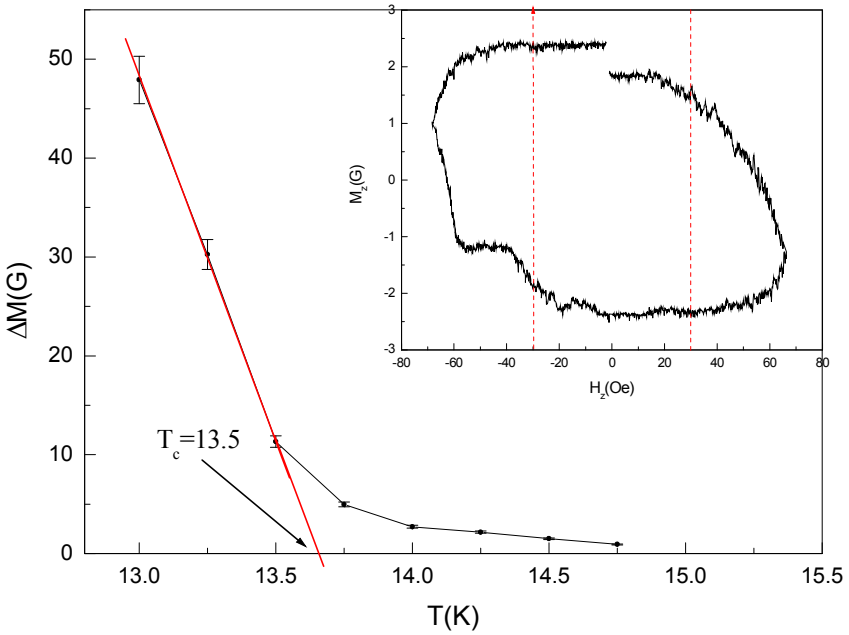

Figure 2 (Colour on-line) Diamagnetic signal estimated from 'local' magnetisation measurements as a function of temperature (see text). The inset shows a typical M_l-H_z hysteresis loop captured at T=12.5K.

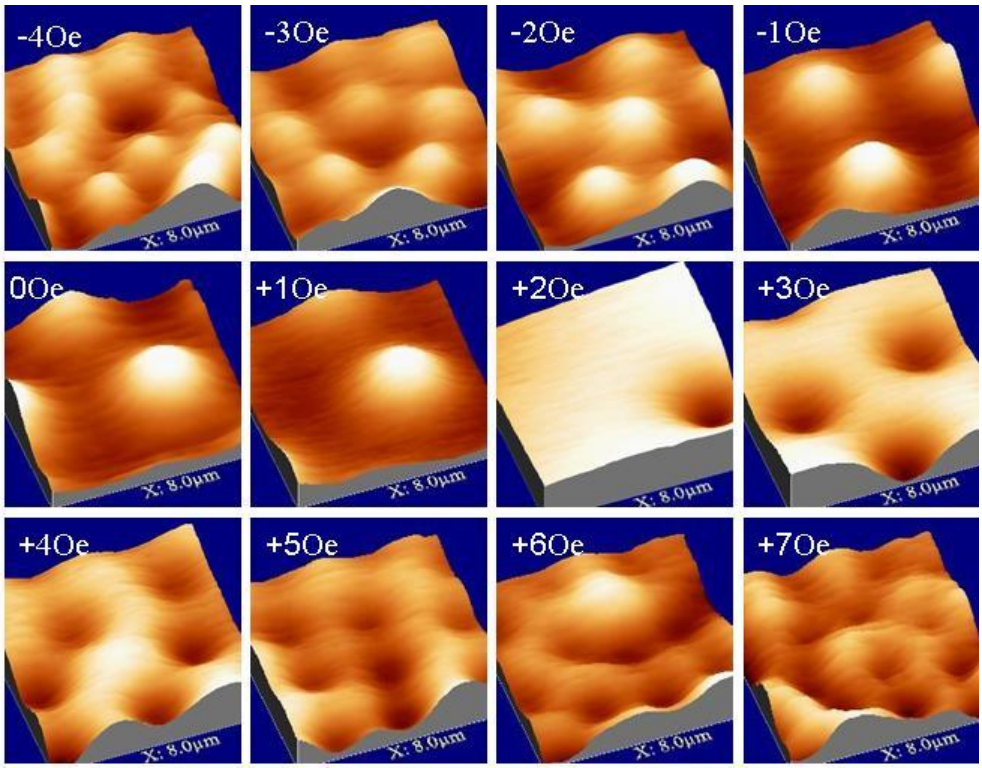

Figure 3 (Colour on-line) Three dimensional scanning Hall probe microscopy images of vortices in a Co-doped $SrFe_2As_2$ single crystal after field-cooling from above T_c to T=8K in various applied magnetic fields. Scan size ~8μm×8μm.

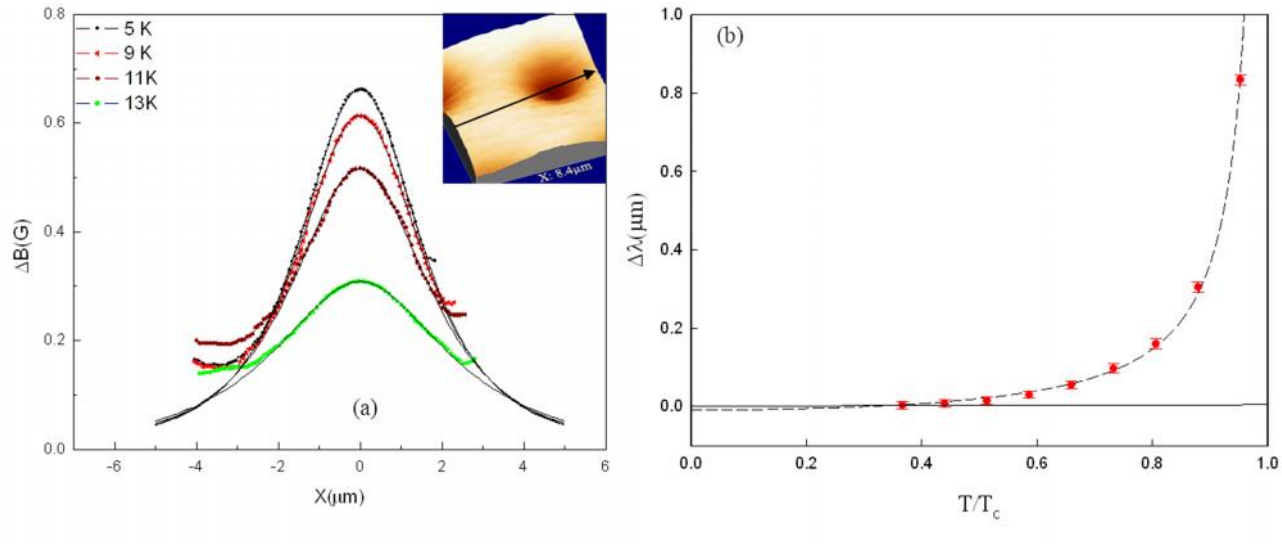

Figure 4(a) (Colour on-line) Magnetic field profiles across a single vortex after field-cooling in H_z=+1Oe to the indicated target temperature. Points are experimental data and solid lines are fits to a modified variational model due to Clem. The insert shows the raw vortex image at T=5K. (b) $\Delta\lambda=\lambda(T)-\lambda(0)$ extracted from the fits as a function of temperature.

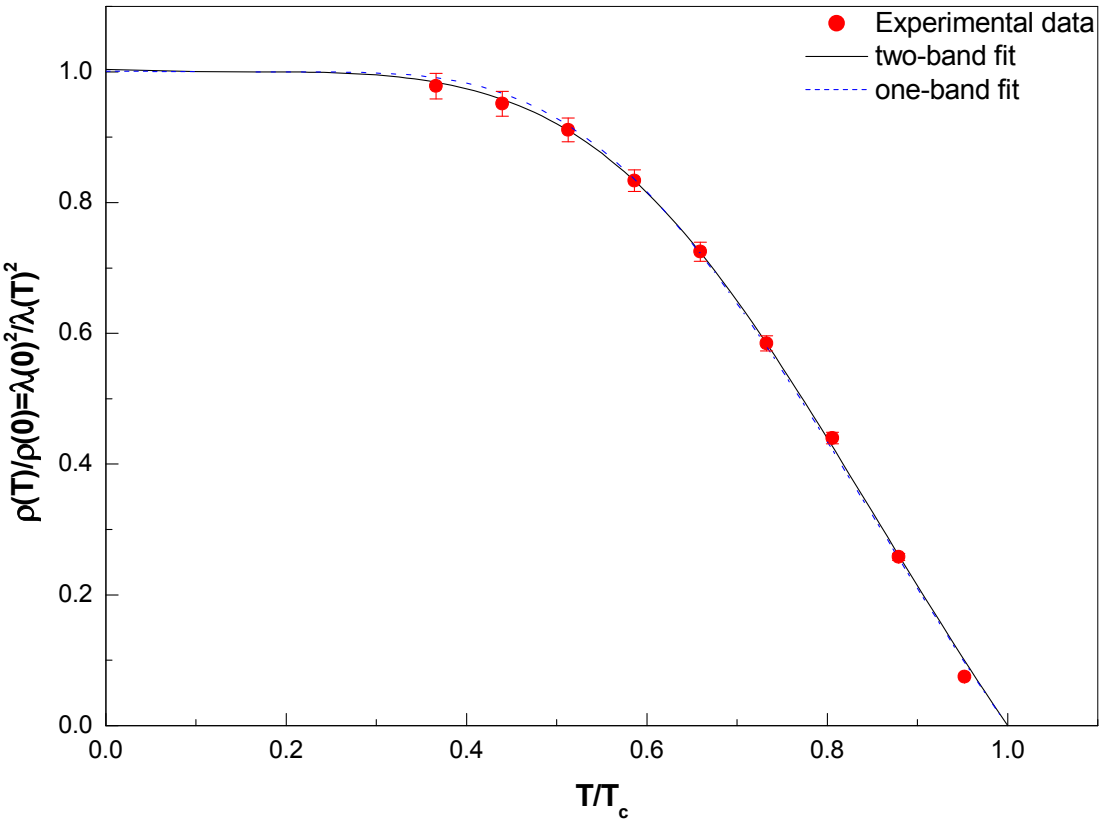

Figure 5 (Colour on-line) Experimentally estimated temperature-dependent superfluid density, ρ_s(T) (points), the results of a two band α-model (solid line), where p=0.49 a_1=0.94 (a_2=1, Δ_1=4.8kT_c, Δ_2=2.0kT_c) and the results of a one band model (dashed line) where a=0.92, Δ =2.81kT_c – see text.

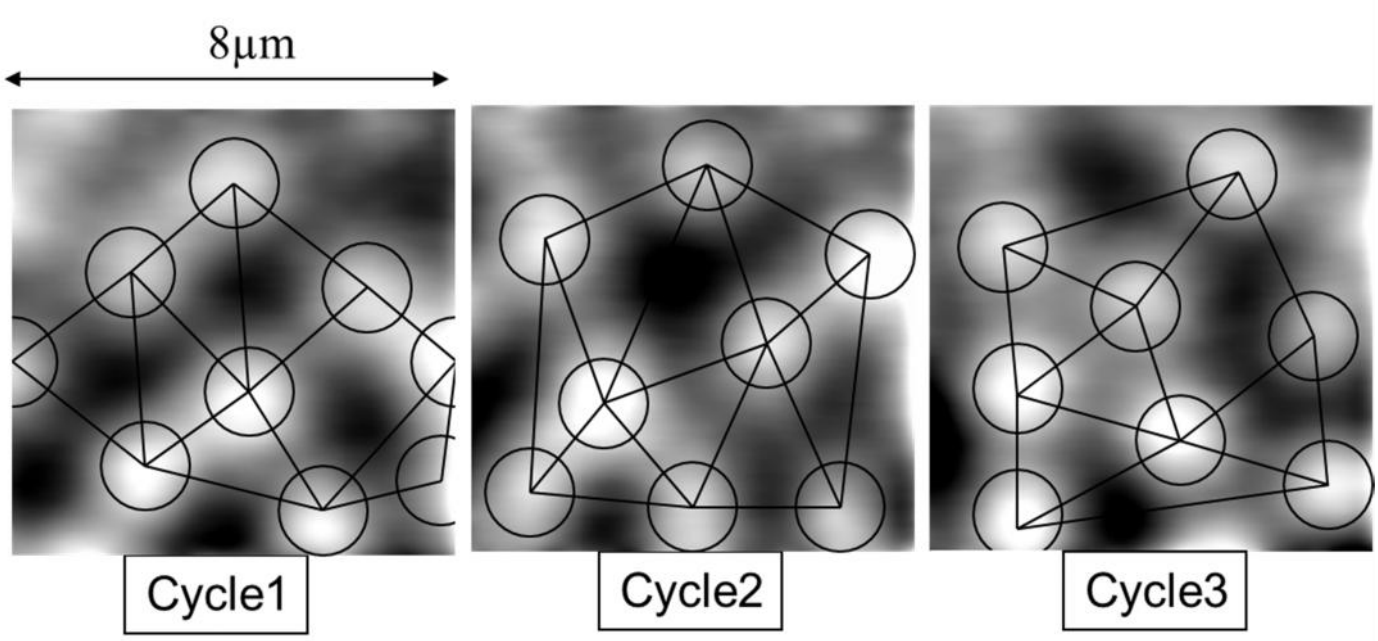

Figure 6 (Colour on-line) Vortex images captured after repeatedly field-cooling the sample from above T_c to T=8K in an applied magnetic field, H_z=+5 Oe.